Preparation, Crystal Structure, Properties, and Electronic Band Structure of $TlTaSe_3$

Christoph L. Teske[a], Wolfgang Bensch[a], Diana Benea[b], Jan Minár[b], Alexander Perlov[b], and Hubert Ebert[b]

[a] Institut für Anorganische Chemie, Christian-Albrechts-Universität, Otto-Hahn-Platz 6/7, D-24098 Kiel, Germany
[b] München, Department Chemie – Physikalische Chemie, Ludwigs-Maximilians-Universität, Butenandtstraße 11, D-81377 München

Reprint requests to Dr. C. Teske. Fax: +49 431 880 1520. E-mail: cteske@ac.uni-kiel.de

Z. Naturforsch. **60b,** 858 – 866 (2005); received June 10, 2005

$TlTaSe_3$ was prepared from a fused mixture of $Tl_4Ta_2Se_{11}$, Ta and Se in the molar ratio 1:2:1. The compound shows dimorphism with H-$TlTaSe_3$, hexagonal, space group $P6_3/mmc$, $a = 7.2436(6)$, $c = 5.9736(6)$ Å, $c/a = 1.213$ and O-$TlTaSe_3$, orthorhombic, space group $Pnma$, $a = 9.554(13)$, $b = 3.6244(6)$, $c = 14.7271(17)$ Å. The crystal structure of H-$TlTaSe_3$ is isotypic to $BaVSe_3$ whereas that of O-$TlTaSe_3$ is closely related to the NH_4CdCl_3-type. Characteristic features of the structures are: $^1_\infty[TaSe_3{}^{2-}]$ chains of regular octahedra sharing faces along [001] for the hexagonal form and columns of double edge-sharing octahedra $^1_\infty[Ta_2Se_6{}^{2-}]$ running along [010] for O-$TlTaSe_3$. The columns are each separated by Tl^+ ions with the coordination number CN = 12 and CN = 8 respectively. The structures are compared and discussed in context with other isotypic structures of chalcogenides. The orthorhombic modification O-$TlTaSe_3$ is a semiconductor while H-$TlTaSe_3$ shows conventional metallic behaviour. The electronic structures of both modifications are discussed on the base of band structure calculations performed within the framework of density functional theory.

Key words: Thallium Tantalum Selenide, Crystal Structure, Dimorphic, Properties, Electronic Band Structure

Introduction

Recently we reported on the preparation, structure and physical properties of $TlTaS_3$ [1]. This compound was prepared by reacting mixtures of Ta powder, Tl_2S and sulphur in sealed glass tubes in a temperature range 445 °C ≤ T ≤ 495 °C. The investigations revealed an orthorhombic structure closely related to the NH_4CdCl_3-type (Strukturberichte, type E24) having columns of double edge-sharing octahedra $^1_\infty[Ta_2Se_6{}^{2-}]$. $TlTaS_3$ is a semiconductor with a narrow optical band gap $E_g \approx 0.78$ eV. In addition, a Nuclear Magnetic Resonance study of ^{203}Tl and ^{205}Tl was carried out [2]. These results show noticeable intra-chain (Tl-Tl) and inter-chain (Tl-Ta) indirect nuclear spin-spin interactions. These findings lead to the question whether the homologous selenide can be prepared and whether it shows the same structural and physical properties. In the present article, results of pertinent experimental and theoretical investigations are presented. In particular, we report on the preparation, structure, electronic band structure, and some physical properties of $TlTaSe_3$.

Experimental Section

Preparation

The starting materials were Ta powder (99,7% Riedel-De Haën AG), $Tl_4Ta_2Se_{11}$ [3] and Se powder (grey, Riedel-De Haën AG). The selenide was prepared from a mixture of appropriate amounts of Ta and Se with $Tl_4Ta_2Se_{11}$ [3] (2:1:1) to give the composition $TlTaSe_3$. This mixture was reacted in a flame-sealed glass (DURAN®) ampoule (argon, reduced pressure) at 480 °C. Starting with a black thin liquid melt the sample began to crystallise after a few hours yielding after four days an anthracite bulk of microcrystalline $TlTaSe_3$. All attempts to prepare single crystals at elevated temperatures suitable for X-ray investigations were not successful. Rising the temperature above approximately 550 °C promotes decomposition as confirmed by X-ray powder diffraction and thermal investigations. Finally, single crystals could be grown from a solution in molten TlBr. A mixture of powdered $TlTaSe_3$ (prepared as mentioned above) and TlBr (mo-

No.	$2\theta_{obs}$	*h*	*k*	*l*	$2\theta_{calc}$	$\Delta 2\theta$	$I_{rel.}$	d_{obs}	d_{calc}
*1	13.940	0	0	2	13.921	0.0189	22.9	6.3477	6.3563
2	14.102	1	0	0	14.107	−0.0047	45.8	6.2753	6.2732
3	20.517	1	0	1	20.514	0.0034	29.6	4.3253	4.3260
4	22.947		?				1.8	3.8725	
5	24.563	1	1	0	24.559	0.0033	75.1	3.6213	3.6218
6	28.429	2	0	0	28.433	−0.0037	4.8	3.1370	3.1366
7	29.893	0	0	2	29.891	0.0021	9.1	2.9866	2.9868
8	30.458		?				1.7	2.9325	
*9	30.899	1	0	1	30.881	0.0180	2.2	2.8916	2.8933
10	31.514		?				1.3	2.8366	
11	32.205	2	0	1	32.208	−0.0035	100.0	2.7773	2.7770
12	32.768		?				4.4	2.7308	
13	33.192	1	0	2	33.196	−0.0027	24.6	2.6969	2.6967
*14	33.223	1	0	2	33.258	−0.0351	19.9	2.6945	2.6917
15	35.517		?				1.2	2.5255	
16	36.225		?				9.9	2.4778	
*17	36.896	1	0	3	36.919	−0.0223	1.4	2.4342	2.4328
18	37.922	2	1	0	37.917	0.0057	12.2	2.3707	2.3710
19	40.924	2	1	1	40.918	0.0065	5.3	2.2034	2.2038
20	41.712	2	0	2	41.725	−0.0132	121.4	2.1636	2.1630
21	43.241	3	0	0	43.231	0.0094	12.8	2.0906	2.0911
22	46.679		?				5.8	1.94443	
23	49.017	2	1	2	49.014	0.0029	8.9	1.8569	1.8570
24	50.346	2	2	0	50.348	−0.0019	24.9	1.8110	1.8109
25	52.552	3	1	0	52.557	−0.0051	7.3	1.7400	1.7399
*26	53.372	1	1	0	53.364	0.0080	3.1	1.7152	1.7155
27	54.190		?				2.6	1.6912	
28	54.552	2	0	3	54.545	0.0073	5.0	1.6809	1.6811
*29	55.443	1	1	2	55.433	0.0100	1.5	1.6559	1.6562
30	57.553		?				0.8	1.6001	
*31	57.995	0	0	8	57.992	0.0026	3.1	1.5890	1.5891
32	59.657	2	2	2	59.662	−0.0056	4.6	1.5486	1.5485

Table 1. X-ray powder diffraction pattern for H-$TlTaSe_3$. Space group and cell parameters see text. (Observed (obs) and calculated (calc) values, d-spacing values, I refers to integrated intensities scaled in percentage of the strongest reflection No. 11. Asterisks (*) indicate the reflections assigned to 2H-$TaSe_2$, zero point (refined): for H-$TlTaSe_3$ $z = 0.0178$, for 2H-$TaSe_2$ $z = -0.0391$).

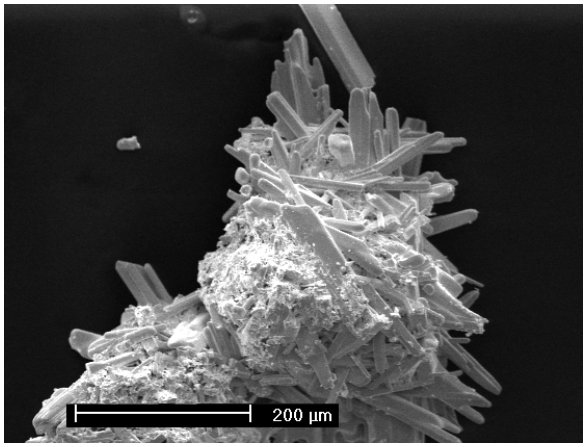

Fig. 1. SEM micrograph of O-$TlTaSe_3$ crystals as grown from a TlBr melt (s. text).

lar ratio 1:1) was filled into in a glass (DURAN®) ampoule (*ca.* 18 cm long). After rinsing with dry argon and evacuation ($p \approx 8$ mbar) it was flame-sealed and placed asymmetrically inside the tube of a horizontally arranged furnace. The one end of it with the mixture was located in the middle of the heating zone while the other end reached just outside the furnace tube. While keeping the temperature of the mixture just above the melting point of TlBr (480 °C), TlBr sublimated to the cooler zone of the glass ampoule. After about three days all TlBr had separated from the mixture leaving behind bunches of slim black shiny crystal needles of $TlTaSe_3$ (Fig. 1). The length L of the needles was in the range of 100 μm $\leq$ L $\leq$ 2 mm. Some of these crystals could be isolated and were suitable for single crystal X-ray structure investigations and also for electrical resistivity measurements. An EDX analysis indicated the presence of the three elements Tl, Ta and Se with an approximate atomic ratio of 1:1:3, and no bromine was detected.

Characterisation

X-ray investigations

X-Ray powder diffraction was carried out on a SIEMENS D5000 diffractometer in the range of $7^\circ \leq 2\theta \leq 60^\circ$ using Cu-K_{α_1} ($\lambda = 1.54056$ Å) radiation. Surprisingly, the powder patterns of the black bulk and that of the crystal needles from the TlBr melt were not identical. The latter resembles that of the homologous sulphide $TlTaS_3$ with orthorhombic sym-

Table 2. Crystal data and structure refinement for O-$TlTaSe_3$[c].

Empirical formula	$TlTaSe_3$
Formula weight	622.20
Temperature	293(2) K
Wavelength	0.71073 Å
Crystal system	orthorhombic
Space group	*Pnma*
Unit cell dimensions	$a = 9.5540(13)$ Å
	$b = 3.6244(6)$ Å
	$c = 14.7271(17)$ Å
Volume	509.96(12) Å^3
Z	4
Density (calculated)	8.10 g/cm^3
Absorption coefficient μ	74.2 mm^{-1}
$F(000)$	1024
Crystal size	$0.3 \times 0.1 \times 0.1$ mm^3
θ-Range for data collection	$2.54^\circ - 30.01^\circ$
Index ranges	$-13 \le h \le 1$,
	$-5 \le k \le 5$,
	$-1 \le l \le 20$
Reflections collected	1764
Independent reflections	852 [R(int) = 0.1085]
Completeness to $\theta = 30.01$	100.0%
Refinement method	Full-matrix least-squares on F^2
Min./max. transm.	0.0025, 0.0252
Data / restraints / parameters	852 / 0 / 31
Goodness-of-fit on F^2	1.064
Final R indices[a,b] $[I > 2s(I)]$	$R_1 = 0.0609$, $wR_2 = 0.1387$
R Indices (all data)[a,b]	$R_1 = 0.0703$, $wR_2 = 0.1457$
$\Delta\rho$ (max./min.)	4.67 / −5.5 eÅ^{-3}

[a] $R_1 = \Sigma||F_o| - |F_c||/\Sigma|F_o|$; [b] $wR_2 = [\Sigma w({F_o}^2 - {F_c}^2)^2 / \Sigma w({F_o}^2)^2]^{1/2}$, $w = 1/[\sigma({F_o}^2) + (aP)^2 + bP]$ where $P = (\max({F_o}^2, 0) + 2 \cdot {F_c}^2)/3$; [c] further details of the crystal structure can be obtained from Fachinformationszentrum Karlsruhe, D-76334 Eggenstein-Leopoldshafen or *via* e-mail crysdata@fiz-karlsruhe.de free of charge upon quoting the number CSD-415528.

Table 3. Atomic coordinates and equivalent isotropic displacement parameters (Å^2) for O-$TlTaSe_3$. $U_{(eq)}$ is defined as one third of the trace of the orthogonalized U_{ij} tensor.

Atom	x	y	z	$U_{(eq)}$
Tl	0.0186(1)	3/4	0.8290(1)	0.038(1)
Ta	0.1617(1)	1/4	0.5702(1)	0.025(1)
Se(1)	0.3177(2)	3/4	0.4979(1)	0.024(1)
Se(2)	0.2537(2)	1/4	0.7204(1)	0.026(1)
Se(3)	0.0287(2)	1/4	0.3993(1)	0.022(1)

metry whereas the first one of the originally prepared sample is totally different and obviously not of a single phase. However, the stronger reflections could be indexed (Table 1) with a hexagonal unit cell, $a = 7.2436(6)$, $c = 5.9736(6)$ Å, $c/a = 1.213$ and $V = 271.44(3)$ Å^3, suggesting the structure is isotypic or closely related to that of $BaVSe_3$ [4]. This was the first evidence for $TlTaSe_3$ being dimorph. In addition, seven of the residual reflections could be assigned to 2H-$TaSe_2$ [5]. The positions of the reflections were compared with those of the theoretical pattern generated from

Table 4. Anisotropic displacement parameters (Å^2) for O-$TlTaSe_3$. The anisotropic displacement factor exponent takes the form: $-2\pi^2[h^2a^{*2}U_{11} + \ldots + 2hka^*b^*U_{12}]$, $U_{12} = U_{23} = 0$.

Atom	U_{11}	U_{22}	U_{33}	U_{13}
Tl	0.036(1)	0.030(1)	0.049(1)	0.002(1)
Ta	0.019(1)	0.026(1)	0.030(1)	−0.002(1)
Se(1)	0.018(1)	0.019(1)	0.033(1)	0.003(1)
Se(2)	0.024(1)	0.026(1)	0.030(1)	−0.003(1)
Se(3)	0.016(1)	0.019(1)	0.031(1)	0.000(1)

Table 5. Selected interatomic distances (Å) for O-$TlTaSe_3$ based on the single crystal data. Estimated standard deviations are given in parentheses.

Tl	Se1	3.191(2) 1×	Se_1	Ta	2.5765(13) 2×
	Se2	3.1965(17) 2×		Tl	3.191(2) 1×
	Se2	3.2998(17) 2×		Tl	3.4526(17) 2×
	Se3	3.393(2) 1×	Se_2	Ta	2.3799(19) 1×
	Se1	3.4526(17) 2×		Tl	3.1965(17) 2×
	Tl	3.6244(6) 2×		Tl	3.2998(17) 2×
Ta	Se2	2.3799(19) 1×	Se_3	Ta	2.6066(12) 2×
	Se1	2.5765(13) 2×		Ta	2.8193(19) 1×
	Se3	2.6066(12) 2×		Tl	3.393(2) 1×
	Se3	2.8193(19) 1×			
	Ta	3.6244(6) 2×			

single crystal data [5] by LAZY Pulverix [6]. The refinement led to $a = 3.431(4)$, $c = 12.713(9)$ Å and $V = 129.6(3)$ Å^3 which is close to the data given by Brown and Beerntsen [5]. The powder pattern was refined with the Rietveld method (FULLPROF 98 [7]) using single crystal data of $BaVSe_3$ [4] (space group $P6_3/mmc$) and of 2H-$TaSe_2$ [5] as the starting models. Convergence was reached with the following R indices [%]: $R_p = 13.1$, R_{wp} 18.9, and $R_{Bragg} = 13.2$, $R_f = 10.4$ for $TlTaSe_3$, and $R_{Bragg} = 9.98$, $R_f = 4.95$ for 2H-$TaSe_2$. All atoms of $TlTaSe_3$ are on special positions and the only free positional parameter x of Se at (6*h*) ($x = 0.1689(5)$) did not change and is identical with that for $BaVSe_3$ within the range of the standard deviation. The Rietveld refinement required a special strategy due to simultaneous occurrence of H-$TlTaSe_3$ and 2H-$TaSe_2$. The reflections of the latter layered compound are ill-shaped and the intensities are rather small. Hence, we decided to treat the powder pattern in the following way. For 2H-$TaSe_2$ only the zero-point and the lattice parameters were refined. The resulting data were fixed in the final Rietveld refinement of H-$TlTaSe_3$. As a consequence of this procedure the zero points (see Table 1) for H-$TlTaSe_3$ and 2H-$TaSe_2$ are different.

The intensity data for single crystal X-ray investigations of orthorhombic $TlTaSe_3$ were collected on a STOE AED II diffractometer (monochromated Mo-K_α radiation; $\lambda = 0.71073$ Å). The space group and the unit cell parameters are *Pnma* (No. 62), $a = 9.554(13)$, $b = 3.6244(6)$, $c = 14.7271(17)$ Å, $V = 509.96(12)$ Å^3, $Z = 4$. A correction for Lorentz, polarisation effects was performed and an absorp-

tion correction was applied using X-Red [8] and X-Shape [9]. Technical details of the data acquisition and some selected results of the refinement are summarised in Table 2. The refinement of the atomic positions taken from the crystal structure of $TlTaS_3$ was done against F^2 employing SHELXL-97 [10]. All atoms were refined with anisotropic displacement parameters. The final atomic coordinates as well as the equivalent isotropic displacement coefficients are listed in Table 3 and anisotropic displacement parameters in Table 4. The shortest interatomic distances in the range of $2.3799\ \text{Å} \leq d_{A-B} \leq 3.6244\ \text{Å}$ are given in Table 5.

Thermal analysis

The samples were flame-sealed in glass (DURAN®) ampoules with dry argon. Differential scanning calorimetry was performed on a DSC-204 device from NETZSCH at heating (cooling) rates of 3 K/min up to $T_{max} = 540$ °C.

Electrical conductivity

For electrical measurements a slim crystal needle (*ca.* 2×0.2 mm) of orthorhombic $TlTaSe_3$ was glued to a copper carrier with insulating resin. Contacts were made with silver conducting paste. The resistance was recorded in the temperature range $50\ \text{K} \leq T \leq 275\ \text{K}$ applying the four-probe method and *dc* mode.

Band structure calculations

Calculations of the electronic band structure have been carried out in the framework of the Local Density Approximation (LDA) to Density Functional Theory [11] using the LMTO-ASA method and including the so-called combined correction terms [12]. As the crystal structure of $TlTaSe_3$ is relatively open, in the case of O-$TlTaSe_3$ so-called empty spheres were introduced to improve the numerical accuracy of the calculations. The calculations were carried out in the semi-relativistic mode, *i.e.* all relativistic effects were taken into account except for the spin-orbit coupling. The angular momentum expansion of the basis functions was made up to $l = 3$ for Tl and $l = 2$ for Ta, Se, and the empty spheres. The *k*-space integration was performed using the tetrahedron method [13] on a grid of 425 k-points in the irreducible part of the Brillouin zone for O-$TlTaSe_3$ and 485 k-points for H-$TlTaSe_3$. From the energy bands and the LMTO eigenvectors total and orbital (l-projected) density of states (DOS) functions were calculated.

Results and Discussion

Preparation

Preparation of single phase $TlTaSe_3$ is complicated by the fact that the stability of Ta^{5+} in the presence of Se decreases with increasing temperature. Above $T \approx 500$ °C the formation of $TaSe_2$ becomes increasingly favoured. Therefore, starting mixtures consisting of the polyselenide $Tl_4Ta_2Se_{11}$(Fp $= 452 \pm 2$ °C) [3], Ta and Se (see above) turned out to be more appropriate for the synthesis of $TlTaSe_3$ than reactions with stoichiometric mixtures of the elements and Tl_2Se. Because of the latter reaction being strongly exothermic it is driving the temperature inevitably above 500 °C for at least some seconds. Overheating of the samples for shorter or longer periods always caused an increase of the amount of $TaSe_2$ (see (*) Table 1). $TlTaSe_3$ can be stored for a reasonably long period in air. According to the DSC experiments orthorhombic $TlTaSe_3$ transforms into the hexagonal form in the temperature range of $490\ ^\circ\text{C} \leq T \leq 520\ ^\circ\text{C}$, which is indicated by a broad endothermic event. On cooling down no further event was detected. The endothermic event did not occur again during the following heating cycles. This indicates that the transition might be irreversible.

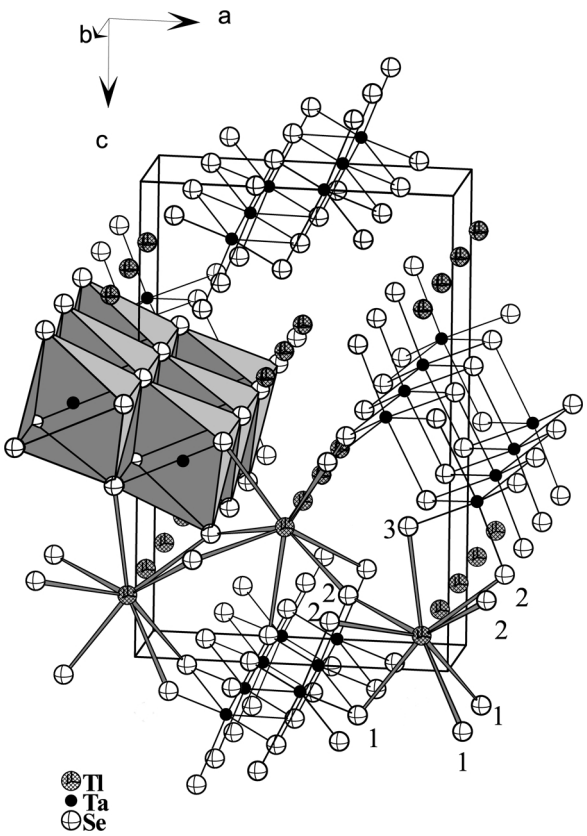

Fig. 2. Crystal structure of O-$TlTaSe_3$. Perspective view along [010]. Some of the $TaSe_6$ octahedra and some Tl-Se-distances are shaded to highlight edge sharing. The numbers refer to the crystallographic sites of the Se-atoms (s. Table 3 and Fig. 3)

Crystal structures

$TlTaSe_3$ is dimorphous crystallising either orthorhombically (O-$TlTaSe_3$) or hexagonally (H-$TlTaSe_3$) depending on the preparative conditions. The orthorhombic form is isostructural with $TlTaS_3$ and isotypic with a number of already known chalcogenides with composition ABX_3 (X = S, Se), as mentioned earlier [1]. The structures of these compounds with large cations A^{n+} are closely related to the NH_4CdCl_3-type (Strukturberichte, type E24). Characteristic features of this structure are columns of double edge-sharing octahedra $^1_\infty[B_2X_6{}^{2-}]$ running along the *b* axis. In O-$TlTaSe_3$ the columns $^1_\infty[Ta_2Se_6{}^{2-}]$ are separated by Tl^+ ions (Fig. 2). The Ta-Se distances are not equivalent (Table 5) with one short bond length of 2.3799(13) Å and one significantly longer with 2.8193(19) Å (average for all 6 Ta-Se bonds: 2.5942(15) Å. The sum of the ionic radii for Ta^{5+} and Se^{2-} [14] corresponds to 2.62 Å for CN = 6. The position of Ta^{5+} is slightly shifted ($d \approx 0.35$ Å) from the plane Se(1)-Se(1)-Se(3)-Se(3) towards Se(2), the unlinked vertex of the octahedron.

The Tl^+ ions are surrounded by eight nearest Se^{2-} forming a distorted bi-capped trigonal prism with Tl^+ in an off-centre position shifted towards the upper edge occupied by two Se(2) atoms (Fig. 3). There are five short Tl-Se(1) bonds ranging from 3.191(2) to 3.2998(17) Å and three significantly longer distances between 3.393(2) and 3.4526(17) Å (Table 5). Such an asymmetric environment was already discussed in detail in context with the homologous sulphide [1] and of some isostructural compounds as *e. g.* $PbZrS_3$ [15]. On the one hand it might be due to the presence of the $6s^2$ lone pair. On the other hand the asymmetry

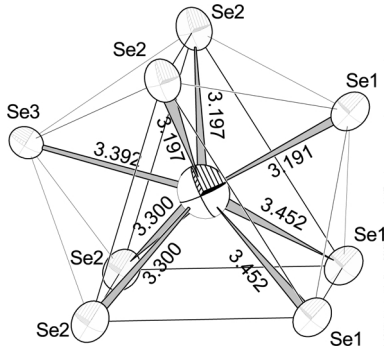

Fig. 3. Coordination polyhedra around Tl^+ in O-$TlTaSe_3$ with atom labelling scheme and interatomic distances Tl-Se. (Displacement ellipsoids are drawn at 95% probability level).

may be caused by the fact that the three Se^{2-} anions contribute in a different way to charge compensation because they are not structurally equivalent. Analogous to the isostructural $TlTaS_3$ the two unique anions $Se(1)^{2-}$ and $Se(2)^{2-}$ are five-coordinated with $Se(1)^{2-}$ being surrounded by two Ta^{5+} and three Tl^+, whereas $Se(2)^{2-}$ has only one Ta^{5+} and four Tl^+ ions as nearest neighbours. The third ion $Se(3)^{2-}$ is four-coordinated by three Ta^{5+} and one Tl^+ (Table 5). We note that $Se(2)^{2-}$ has the shortest average distance to the Tl^+ ions giving a better charge compensation (average Tl-Se(2) = 3.2482(17) Å; for comparison: average Tl-Se(1) = 3.3654(18) Å).

Further influence of the size and charge of A^{n+} atoms without lone pairs or of the X atoms (X = S, Se) in ABX_3 can be recognized by comparison with the structures of other ternary chalcogenides. For example, $LaCrSe_3$ [16] and $EuZrSe_3$ [17] adopt the NH_4CdCl_3-type structure but compounds like $AZrS_3$ (A = Ca, Sr, Eu, and Ba) crystallise in distorted perovskite-type structures [18]. Finally, the homologous chalcogenides $CsTaX_3$ (X = S, Se and Te) [19] with the large Cs^+ ion crystallise in the $BaVS_3$-type. In this context the mutual interplay of ion size and charge becomes meaningful again. The formal substitution of S by the larger Se results in dimorphism for $TlTaSe_3$. It can adopt both the orthorhombic and the hexagonal structure type.

With our present X-ray data we cannot exclude a disorder of the Ta^{5+} position in H-$TlTaSe_3$. In the case of $CsTaX_3$ [19] Ta^{5+} is displaced from the centre of the base of the octahedron in the [001] direction. However, between the orthorhombic and hexagonal structures of $TlTaSe_3$ some fundamental differences should be noted. In the structure of H-$TlTaSe_3$ the thallium atoms are in a 12-fold anti-cuboctahedral coordination with Se^{2-} at Tl-Se distances of 3.629(5) (6×) and 3.630(8) Å (6×). The sum of the ionic radii [14] for Tl^+ and Se^{2-} corresponds to 3.68 Å. Ta^{5+} has a regular octahedral surrounding of Se^{2-} (Ta-Se: 2.593(9) Å) provided there is no displacement. The octahedra share faces to form $^1_\infty[TaSe_3^{2-}]$ chains running in the [001] direction (Fig. 4). The Ta-Ta distances along the chains of 2.987(5) Å are about 17% shorter than in O-$TlTaSe_3$ (Ta-Ta: 3.6244(6) Å). The packing of the ions in O-$TlTaSe_3$ is closer than in H-$TlTaSe_3$ with molar volumes of 76.8 cm^3 for O-$TlTaSe_3$ and 81.7 cm^3 for H-$TlTaSe_3$. Thus, the density of the orthorhombic form is higher (8.1 g/cm^3) than that of the hexagonal modification (7.62 g/cm^3), and the mean Tl-Se distance of

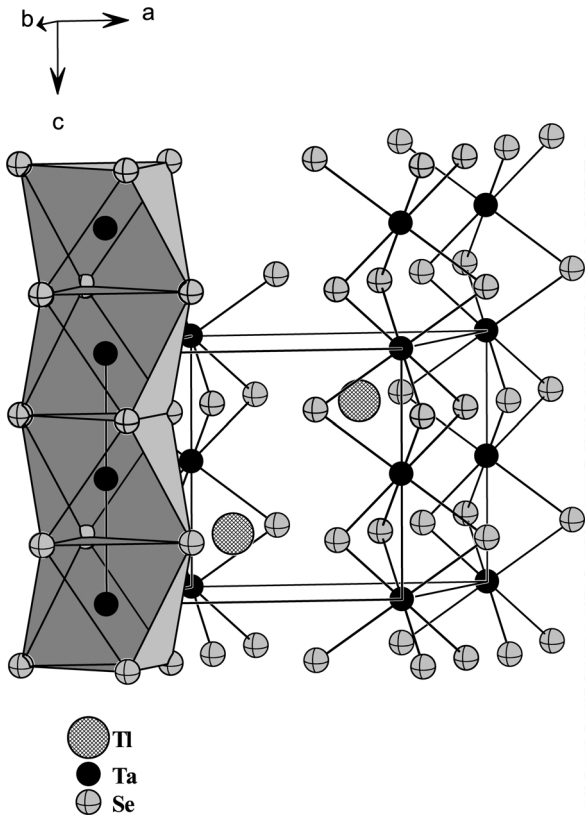

Fig. 4. Crystal structure of H-$TlTaSe_3$. Perspective view along [010]. Some of the $TaSe_6$ octahedra are shaded to highlight face sharing along [001].

3.3105(18) Å in O-$TlTaSe_3$ is significantly shorter than in H-$TlTaSe_3$ of 3.626(7) Å.

Conductivity and electronic structure

O-$TlTaSe_3$ is a semiconductor (see Fig. 5a) as the sulphide $TlTaS_3$ [1]. Fig. 5b shows the semi-logarithmic plot of the relative conductivity $\sigma_{(T)} = R_{298}/R_{(T)}$ (R_{298}: resistivity at room temperature, R: actual resistivity for temperature T) against reciprocal temperature ($1/T$). In the lower temperature region from 71 to 154 K a linear dependency of $\ln(\sigma)$ on $1/T$ is observed. From this plot an activation energy of $E_a \approx 0.149(2)$ eV can be estimated. Taking into consideration thermal excitations between impurity states located just above the top of the valence band (VB) and below the bottom of the conduction band (CB) such a low value of E_a is not surprising. Applying the same equation ($-E_a = m \times 2k\,T$, m = slope, k = 0.0862 eV/T, T/K) to the data of $TlTaS_3$

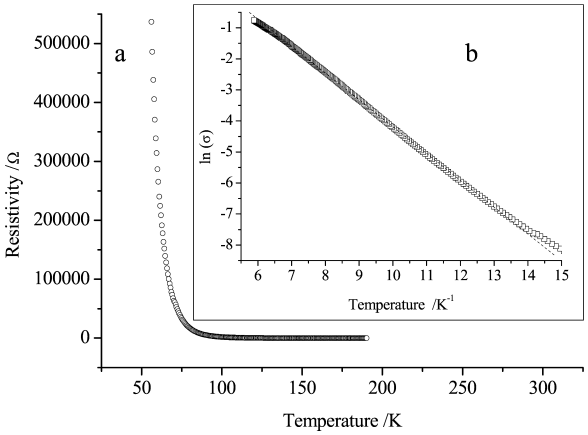

Fig. 5. Electrical properties of O-$TlTaSe_3$. Fig. 5a shows the resistivity as a function of the temperature. Fig. 5b is a semi-logarithmic plot of the relative conductivity (σ) against the reciprocal temperature (slope of the linear part, $m = -0.8649(12)$).

in the lower temperature region we find a somewhat larger value of $E_a \approx 0.175$ eV. For the sulphide the optical band gap was estimated to $E_g \approx 0.78$ eV [1]. For $TlTaSe_3$ the diffuse UV/Vis reflectance spectra (Diffuse Reflectance Accessory Cary 5) could not be recorded because no significant signal was detected in the region of low energy (250 to 2000 nm). However, the width of the optical band gap should be significantly smaller than 0.78 eV.

The theoretical electronic band structure

In the contrast to the experimental finding our LDA-based band structure calculations for O-$TlTaSe_3$ led to a semi-metallic behavior, *i.e.* the VBs and CBs slightly overlap as could be seen from an inspection of the dispersion relation E(k). This inconsistency which is obviously caused by a shortcoming of LDA, could be removed by a slight increase of the lattice parameter. The total as well as component and angular momentum resolved density of states (DOS) curves obtained by a lattice expansion of 2% are shown in Fig. 6. As can be seen from these results the main contribution to the DOS in the VB regime from about -6 eV up to the Fermi level stem from Se *p*-, Tl *s*-, *p*- and Ta *d*-states. The fact that none of the components strongly dominates in this energy regime reflects the primary covalent nature of the interatomic bonds in O-$TlTaSe_3$. In this context it is interesting to note that the Ta *d*-states give a relatively large contribution in contrast to

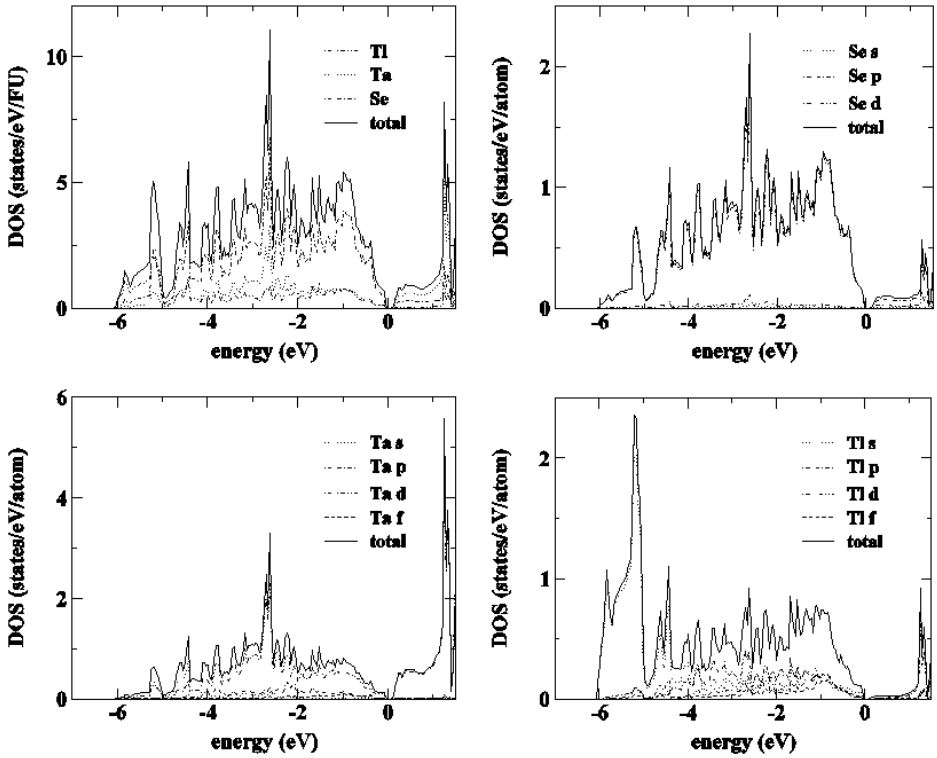

Fig. 6. Calculated total density of states curve (DOS) together with the angular momentum resolved partial DOS curves for O-$TlTaSe_3$.

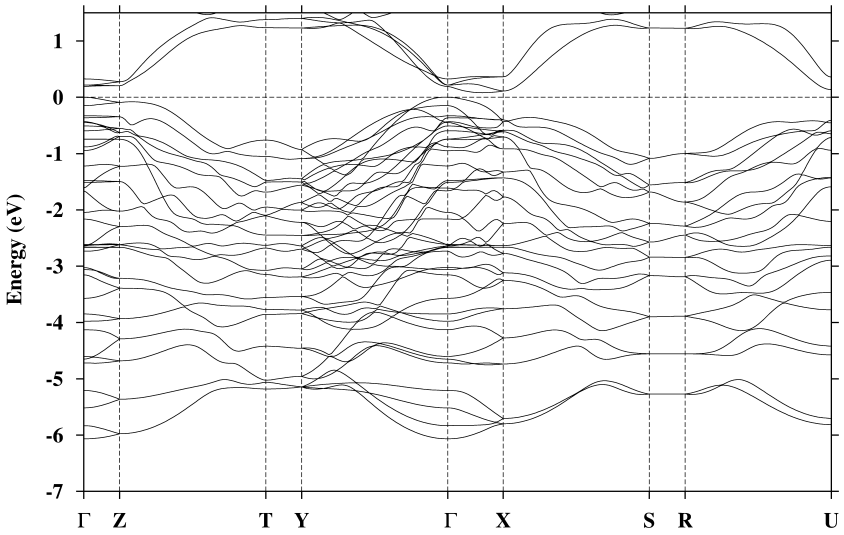

Fig. 7. The E(k) relation for O-$TlTaSe_3$.

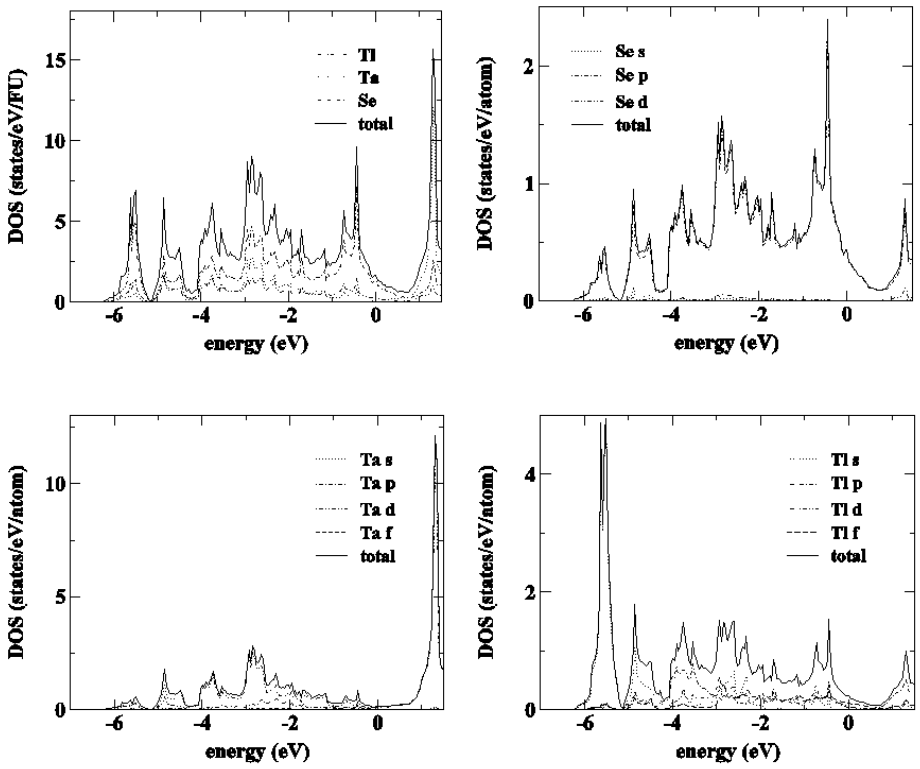

Fig. 8. Total DOS (top, left), Se contribution (top, right), Ta contribution (bottom left) and Tl contribution (bottom, right) in H-$TlTaSe_3$.

a naive formal valence consideration that would lead to a Ta 5*d*0 electronic configuration. The Tl states form a relatively narrow sub-band at the bottom of the VB between -6 and -4 eV which shows only a weak hybridisation with the Se *p*-states. In addition there is a narrow semi-core band between -14 and -12 eV (not shown in Fig. 6) which originates from Se 3*s*-state. Accordingly, this band shows very little hybridization with the Tl and Ta derived states. Finally, the CB is dominated by Ta *d*- and Tl *p*-states which mix with the Se *p*- and *d*-states.

A more detailed insight in the chemical bonding and in particular its anisotropy is supplied by the dispersion relation E(k) of O-$TlTaSe_3$ which is shown in Fig. 7. As indicated above, O-$TlTaSe_3$ is a semiconductor with an indirect gap, with the top of the VB at the Γ point. Accordingly, the bands along Γ-X and Γ-Z are just below the Fermi level while those along X-S, R-U and Z-T are significantly below E_f. In the latter case a pronounced dispersion is found that gives clear evidence for strong bonding interactions for the atoms along the chain direction. Neighbouring chains are connected by the Tl+ ions. The short Tl-Se distances with 3.191(2) and 3.2998(17) Å accordingly give rise to an appreciable dispersion along Γ-X. On the other hand, the Tl-Se bonds along the *z*-axis, *i.e.* parallel to Γ-Z, are longer and as a consequence the bands lie further below and show clearly less dispersion than along Γ-X.

Our results for the total and component angular momentum resolved DOS curve for H-$TlTaSe_3$ are shown in Fig. 8. In contrast to the orthorhombic polymorph the hexagonal compound shows without any doubt a clear metallic behavior. There is in particular an energy overlap of the VBs and CBs such that the Fermi level is crossed by various bands connecting the VB and CB regimes. As Fig. 8 shows, the main contribution to the DOS at E_f comes from Se *p*-states which are mixed with Tl *s*- and Ta *d*-states. As in O-$TlTaSe_3$ between -6 eV and the Fermi level the VB is primarily derived from Se *p*-, Tl *s*-, *p*- and Ta *d*-states. Again, the Tl *s*-states form a relatively narrow band at the bottom of the VB regime between -6 and -4 eV showing only weak hybridization with the Se *p*-states. The narrow semi-core band between -14 and -12 eV stemming primarily from the Se 3*s*-states has only very small contributions from Tl and Ta states. Finally, the CB,

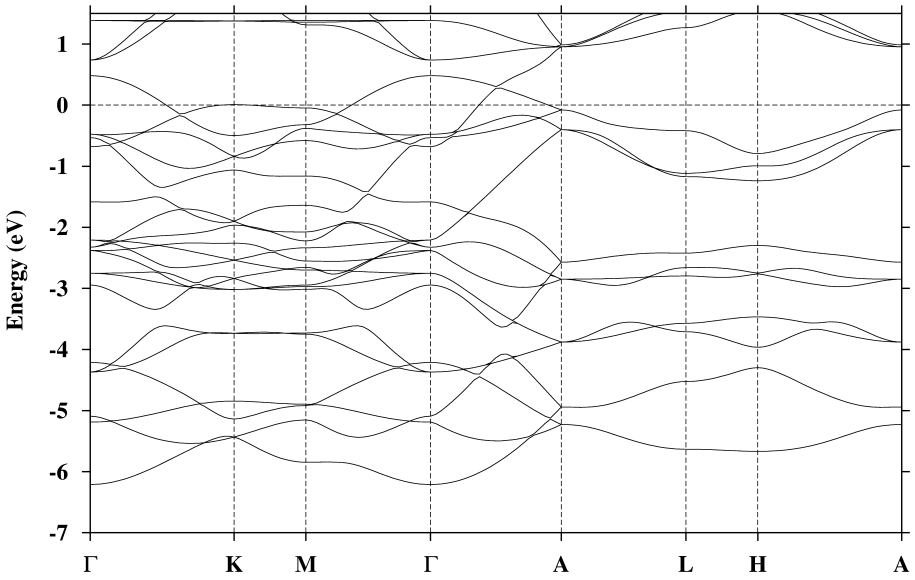

Fig. 9. The E(k) relation for H-$TlTaSe_3$.

the regime above the Fermi energy, is dominated by Ta *d*- and Tl *p*-states which are mixed with Se *p*- and *d*-states. As mentioned above, H-$TlTaSe_3$ shows a conventional metallic behavior with several bands crossing the Fermi level (see Fig. 9). The pronounced dispersion of the band along Γ-A may be explained on the basis of Ta-Ta interactions along the chains due to a relatively short Ta-Ta distance along the atomic chains in the hexagonal structure. Additional Fermi level crossings occur along Γ-K and Γ-M. The dispersion of these bands seems to indicate a non-negligible inter-chain interaction. This is quite surprising as the mean Tl-Se distance (3.626(7) Å) is larger than for O-$TlTaSe_3$ (3.3105(18) Å).

Acknowledgement

We thank I. Jess for the acquisition of the single crystal data.

[1] C. L. Teske, W. Bensch, A. Perlow, H. Ebert. Z. Anorg. Allg. Chem. **628**, 1511 (2002).
[2] A. M. Panich, C. L. Teske, W. Bensch, A. Perlow, H. Ebert, Solid State Commun. **131**, 201 (2004).
[3] C. L. Teske, N. Lehnert, W. Bensch, Z. Anorg. Allg. Chem. **628**, 2651 (2002).
[4] J. Kelber, A. H. Reis (Jr.), A. T. Aldred, M. H. Mueller, O. Massenet, G. Depasquali, G. D. Stucky, J. Solid State Chem. **30**, 357(1979).
[5] B. E. Brown, D. Beerntsen, Acta Crystallogr. **18**, 31 (1965).
[6] K. Yvon, W. Jeitschko, E. Parthé, J. Appl. Crystallogr. **10**, 73 (1977).
[7] J. Rodriguez-Carvajal "Rietveld, Profile Matching & Integrated Intensity Refinement of X-Ray and/or Neutron Data" Version 0.2 1998, Laboratoire Leon Brillouin (CEA CNRS), juan@bali.saclay.cea.fr.
[8] Stoe & Cie, X-Red32 V 1.11 Software; Stoe & Cie GmbH: Darmstadt, Germany (1998).
[9] Stoe & Cie, X-Shape V 1.03 Software; Stoe & Cie GmbH: Darmstadt, Germany (1998).
[10] G. M. Sheldrick, SHELXL-97, Program for the Refinement of Crystal Structures, Univ. Göttingen, Germany (1997).
[11] U. von Barth, L. Hedin, J. Phys. C **5**, 1629 (1972).
[12] O. K. Andersen, Phys. Rev. B**12**, 3060 (1975).
[13] P. E. Blöchl, O. Jepsen, O. K. Andersen, Phys. Rev. B**49**, 16223 (1994).
[14] R. D. Shannon, Acta Crystallogr. **A32**, 751 (1976).
[15] R. Lelieveld, D. J. W. Ijdo, Acta Crystallogr. **B34**, 3348 (1978).
[16] N. Huy-Dung, J. E. Etienne, P. Laruelle, Bull. Soc. Chim. Fr. 2433 (1971).
[17] A. Mar, A. J. Ibers, Acta Crystallogr. C**48**, 771 (1992).
[18] R. Lelieveld, D. J. W. Ijdo, Acta Crystallogr. B**36**, 2223 (1980).
[19] M. A. Pell, G. V. M. Vajenine, J. A. Ibers, J. Am. Chem. Soc. **119**, 5186 (1997).